IEEE Access
Multidisciplinary | Rapid Review | Open Access Journal

Received March 21, 2020, accepted April 3, 2020, date of publication April 28, 2020, date of current version May 15, 2020.

Digital Object Identifier 10.1109/ACCESS.2020.2990870

Joint-SRVDNet: Joint Super Resolution and Vehicle Detection Network

MOKTARI MOSTOFA[1], (Student Member, IEEE), SYEDA NYMA FERDOUS[1], BENJAMIN S. RIGGAN[2], (Member, IEEE), AND NASSER M. NASRABADI[1], (Fellow, IEEE)

[1]Lane Department of Computer Science and Electrical Engineering, West Virginia University, Morgantown, WV 26506, USA
[2]Department of Electrical and Computer Engineering, University of Nebraska–Lincoln, Lincoln, NE 68588, USA

Corresponding author: Moktari Mostofa (mm0251@mix.wvu.edu)

ABSTRACT In many domestic and military applications, aerial vehicle detection and super-resolution algorithms are frequently developed and applied independently. However, aerial vehicle detection on super-resolved images remains a challenging task due to the lack of discriminative information in the super-resolved images. To address this problem, we propose a Joint Super-Resolution and Vehicle Detection Network (Joint-SRVDNet) that tries to generate discriminative, high-resolution images of vehicles from low-resolution aerial images. First, aerial images are up-scaled by a factor of 4x using a Multi-scale Generative Adversarial Network (MsGAN), which has multiple intermediate outputs with increasing resolutions. Second, a detector is trained on super-resolved images that are upscaled by factor 4x using MsGAN architecture and finally, the detection loss is minimized jointly with the super-resolution loss to encourage the target detector to be sensitive to the subsequent super-resolution training. The network jointly learns hierarchical and discriminative features of targets and produces optimal super-resolution results. We perform both quantitative and qualitative evaluation of our proposed network on VEDAI, xView and DOTA datasets. The experimental results show that our proposed framework achieves better visual quality than the state-of-the-art methods for aerial super-resolution with 4x up-scaling factor and improves the accuracy of aerial vehicle detection.

INDEX TERMS Aerial images, multi-scale generative adversarial network (MsGAN), super-resolution, vehicle detection.

I. INTRODUCTION

Real-time vehicle detection in aerial imagery has been an active research area in recent years [1]–[4]. Due to high altitudes in which aerial images are acquired, targets of interest (e.g., vehicles) contain fewer pixels than targets imaged at considerably lower elevations (e.g., building surveillance cameras, or traffic cameras), which significantly degrades detection performance. Moreover, complex background and computational constraints further hinder detection performance. Single image super-resolution (SISR) techniques are commonly used to alleviate poor detection performance by generating a high-resolution counterpart to the original low-resolution image. Recently, generative adversarial networks (GANs) [5] have demonstrated the ability to synthesize high-quality images [6], [7] for many applications, including super-resolution. However, GANs have also been known to be somewhat unstable, frequently lacking discriminability in synthesized imagery. Therefore, we aim to produce and simultaneously train both discriminative and super-resolved images by using multi-task learning to combine correlated tasks such as super-resolution and object detection networks.

The inter-relationship between super-resolution techniques and object detection algorithms has been previously studied to improve detection performance [2], [8], [9]. However, none of them have tried to explore performance of super-resolution if the entire network is trained jointly. One might presume that the reason there are still misdetections and detection failures is because the super-resolution algorithm is not optimized for target detection task.

In this paper, we propose a deep neural network (DNN) framework to simultaneously generate super-resolved aerial images and locate vehicles in the super-resolved images. Our proposed framework is composed of (i) a Multi-scale Generative Adversarial Network (MsGAN) framework to create super resolved versions of the original images. This network preserves high-level features when mapping between low resolution to high resolution domains, and (ii) locate vehicles

The associate editor coordinating the review of this manuscript and approving it for publication was Jon Atli Benediktsson.

This work is licensed under a Creative Commons Attribution 4.0 License. For more information, see https://creativecommons.org/licenses/by/4.0/

using one of the variants of YOLO [10] introduced in [11] as YOLOv3 object detector. We jointly train the entire network at each iteration such that target regions in the super-resolved images become contextually more distinctive from the background. We refer to our proposed algorithm in this paper as the Joint Super-Resolved Vehicle Detection Network (Joint-SRVDNet). Our proposed framework has been evaluated on several extensively used aerial datasets. We train the model on VEDAI, xView and DOTA datasets to evaluate both qualitative and quantitative performances. Moreover, our network shows promising performances compared to a set of state-of-the-art methods. In summary, the key contributions of this paper are as follows:

- In this paper, we propose an end-to-end jointly trainable deep neural network what we named Joint-SRVDNet, which offers a multi-tasking paradigm by handling both super-resolution and vehicle detection for aerial and satellite imagery. To the best of our knowledge, our proposed Joint-SRVDNet is the first multi-task model that leverages complementary information of the two tasks to jointly learn Super-Resolution (SR) and vehicle detection in aerial images. Such a novel framework allows for improved super-resolution reconstructions and more accurate vehicle detection in aerial imagery.
- An MsGAN architecture is proposed for the first time for aerial and satellite image super-resolution, which ensures progressive learning of the statistical distributions of images at multi-scale and significantly improves the performance of SR reconstruction by producing discriminative and high-quality super-resolved images.
- The proposed MsGAN architecture for super-resolution has potential contributions to vehicle detection in low-resolution aerial and satellite images.
- We show remarkable improvements for both super-resolution and vehicle detection for low-resolution aerial imagery with comparable performance to the existing state-of-the-art methods when evaluated on the corresponding high-resolution aerial images.

The rest of this paper is organized in the following manner. Section II reviews related super-resolution and detection algorithms. It also describes challenges when applied to aerial imagery. We give details of our proposed method in section III. Besides, we also discuss the training loss functions of our network in section IV. Section V presents the datasets and experimental details of our work. Section VI shows comparative results and explains the performance. Finally, we provide a conclusion and state some limitations of our algorithm in section VII.

II. RELATED WORK

A. DEEP LEARNING BASED SINGLE IMAGE SUPER-RESOLUTION

Single Image Super-Resolution (SISR) techniques have been studied extensively in the field of computer vision. Recently, Convolutional Neural Network (CNN) architectures have been widely used in image SR algorithms since they can extract representative features that are useful in recovering high-frequency details in super-resolved images. A three-layer CNN was first proposed by Dong *et al.* [12] and referred as SRCNN to learn a mapping between Low-Resolution (LR) and High-Resolution (HR) image pairs, which was later modified in VDSR [13] and DRCN [14]. In VDSR [13], Kim *et al.* implemented an efficient SSIR method, where they showed that increasing the network depth trained by adjustable gradient clipping resulted in a significant improvement in visual quality of super-resolved images. In DRCN [14], they increased recursion depth by adding more weight layers with skip connection to improve the performance of SRCNN. However, all these methods apply interpolation to the LR inputs, which significantly loses some useful information and thereby yields poor results with increased computational cost. Since then these super-resolution architectures have been frequently modified by developing CNN-based architectures like Residual Networks (ResNet) [15], Recurrent Neural Networks (RNNs) [16]–[18] to extract features from the original LR inputs.

Recently, GANs [5] have replaced these SR algorithms. Ledig *et al.* [6] introduce ResNet as the base architecture for image super-resolution and utilize the idea of GAN to reconstruct fine texture details in the super-resolved images. GAN architectures have successfully attained superior performances in many applications of computer vision, such as style transfer, image reconstruction and image SR. SRGAN [6] is the first attempt which utilizes GAN to produce photo-realistic natural looking images close to the original high resolution images. They formulate a loss function which is a combination of a perceptual similarity loss [19]–[21] in addition to an adversarial loss [5] so that the network learns to preserve content of images during SR training. Although SRGAN has shown remarkable performances, still it finds difficulty in generating high-resolution (e.g., 256×256) images due to training instability and mode collapse. During upscaling the LR images to the desired HR counterparts, GAN suffers from the training instability due to low chance of sharing hyper-parameters between image distribution and model distribution in a high-dimensional space. To stabilize the training process, Zhang *et al.* proposed StackGAN [22]. The motivation came from the observation that image distributions are related at multiple scales. StackGAN outperforms significantly other state-of-the-art methods in reconstructing real looking super-resolved images. In StackGAN, they used multiple-generators along with discriminators at each scale to share most of their parameters across the whole network. This structure pushes the resulting solutions towards the original image distributions. For our work, we incorporate the idea of using multiple discriminators at each different scale in addition to the work of Ledig *et al.* [6] where the authors use a perceptual loss function with Mean Squared Error (MSE) loss to generate more realistic SR images. Our network can be viewed as multi-scale GAN architecture since we are using only one generator instead of multiple generators like

StackGAN and stack discriminators at each intermediate outputs to improve the learning of image distributions at multiple scales. As shown in Fig. 2, discriminators at intermediate outputs sequentially help generator produce real-looking super-resolved images to the desired size. The prime goal is to approximate highly related image distributions at different scales. So, stacking multiple discriminators helps the network accomplish this goal by continuously giving feedback from image distributions at one scale to another.

B. DEEP LEARNING BASED VEHICLE DETECTION ARCHITECTURES

Vehicle detection recently has become a prominent research area with applications in civilian and military surveillance, traffic monitoring and planning transportation systems. In [23], the authors proposed a method which utilized Bayesian network to integrate the important features for car detection. Choi and Yang [24] applied the Mean-shift algorithm to extract car like shape for detecting cars in satellite images. In the work of [25], they trained a Dynamic Bayesian Network (DBN) to preserve region level features.

Carlet and Abayowa [26] proposed a modified YOLOv2 [27] for locating vehicles in aerial imagery. A modified faster R-CNN was applied in the work of Terrail and Jurie [28] that showed promising performances in aerial vehicle detection. In [29], Soleimani *et al.* proposed a text-guided detection scheme using both visual and textual features for detection. Yang *et al.* [30] applied skip connection in their framework to merge lower and higher level features and utilized a focal loss function for vehicle detection. For multi-oriented vehicle detection, Deng *et al.* [31] designed a rotatable region proposal network which learned the orientation of vehicles while performing classification on aerial images and videos.

Vehicle detection in overhead imagery remains a challenging issue due to the low resolution of vehicles. To alleviate this shortcoming, researchers have focused on super-resolution techniques. An overview of detection performance on super-resolved images is reported in [8] considering multiple-resolutions. In this paper, we propose a joint training approach which learns to extract discriminative features from low-resolution images such that it can produce super-resolved images that are as visually similar to the corresponding high-resolution images as possible.

C. JOINT TRAINING OF SUPER-RESOLUTION AND DETECTION

Improving object detection performance guided by learning based super-resolution has been a recent research focus. In [8], the impact of super-resolution on object detection has been extensively studied. Haris *et al.* [32] adopt a task-driven super resolution approach employing a novel compound loss based end-to-end training that enhances the image quality leading to a better recognition. Ataer-Cansizoglu *et al.* [33] design an identity preserving face super-resolution framework and achieve outstanding performance for face verification in real time. In this work, the authors propose to use a two-stage loss minimization technique rather than end-to-end training. They hypothesize that end-to-end training involves higher computational complexity respect to limited data samples. On the other hand, another study in [34] propose a deep model that jointly optimizes face hallucination and verification loss for low resolution face identification. In this study, face hallucination loss is measured in terms of pixel difference between the ground truth HR images and network-generated images and verification loss is estimated by the classification error and intra-class distance. Most of the recent works focus on verification, which is easier from the detection task. For example, verification confirms identity whereas detection involves recognition of desired object (e.g., human face, vehicle, etc.). Again, during verification, the probe face has already been detected, but detection has to minimize different constraints before detecting the target object.

Pang *et al.* [35] introduce JCS-Net that combines classification and super-resolution task as one for small-scale pedestrian detection. However, these algorithms do not deal with vehicle detection and super-resolution for aerial imagery that deals with more fundamental challenges. For instance, the average height of pedestrians in the benchmark datasets (e.g., Caltech [36], KITTI [37]) ranges from 60 pixels tall to 430 pixels tall, whereas the average resolution for aerial vehicles is 10×15 pixels in the publicly available benchmark datasets (e.g., VEDAI [38], xVIEW [39], DOTA [40]), which yields poor detection results.

These reviews strongly suggest to use super-resolution technique for developing a robust detection system, which helps to recover detailed information in the low-resolution space. In this paper, we try to investigate the relationship between super-resolution and vehicle detection by proposing a joint training approach so that they can be benefited from each other. We propose to integrate both super-resolution and detection network together. Usually, the super-resolution technique recovers useful detailed information in the low-resolution image, but here it focuses especially on the target regions as detector loss is integrated to SR training. The network gradually learns the input image distributions in the high-resolution space and produce super-resolved version of low-resolution image with distinctive properties of target objects, which also helps detector to achieve better results.

III. PROPOSED FRAMEWORK

In this section, we describe our proposed framework in detail. The proposed framework is an end-to-end network that generates super-resolved aerial images using an MsGAN architecture and jointly optimized YOLOv3 detector to perform vehicle detection in aerial super-resolved imagery.

A. GENERATIVE ADVERSARIAL NETWORKS (GANs)

GANs are a special type of generative models which have shown remarkable performances in representation learning and synthesized image generation. They have been widely

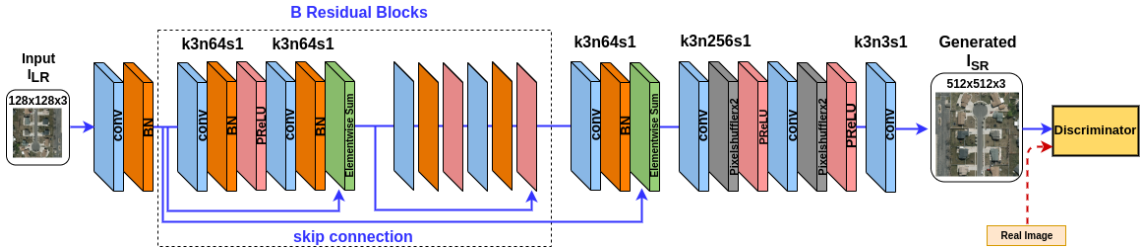

FIGURE 1. Architecture of SRGAN with corresponding kernel size (k), number of feature maps (n) and stride (s) indicated for each convolutional layer.

used in image super-resolution (first applied by Ledig *et al.* in [6]), image synthesis and image translation using conditional GANs (cGANs) [41] and cyclic GANs (cycle-GANs) [7]. Their goal is to learn statistical distribution of the training data to train a mapping $G : x \rightarrow y$ such that image distribution from $G(x)$ is indistinguishable from image distribution of target y. Typically, the generator G is a differentiable function which is trained to learn the distribution p_{data} over data y. To do so, it takes input from the distribution $p_x(x)$ and maps it to the target data space as $G(x; \theta_g)$ where θ_g defines the parameters of the generator model. In addition, the discriminator D acts like a classifier which is trained to return probability distributions $D(y)$ and $D(G(x))$ for both training examples from the distribution $p_{data}(y)$ and samples from $G(x)$, respectively. Basically, D is trained to maximize the probability of assigning the correct label to both training examples and samples from G. Simultaneously G is trained to minimize $log(1 - D(G(x)))$. In other words, D and G play the following two-player minimax game with the adversarial loss $l_{GAN}(G, D)$:

$$\min_G \max_D l_{GAN}(G, D) = \min_G \max_D [E_{y \sim p_{data}}[logD(y)] + E_{x \sim p_x}[log(1 - D(G(x)))]]. \quad (1)$$

However, it is very difficult to achieve the desired output by training the network only with adversarial loss. Adding a l_{L1} reconstruction loss in addition to adversarial loss may result in high quality super-resolved images. Thus, the final objective function consists of two loss function as follows:

$$G^* = arg \min_G \max_D l_{GAN}(G, D) + \lambda l_{L1}(G), \quad (2)$$

where $l_{L1}(G) = \frac{1}{N} \sum_{i=1}^{N} ||y_i - G(x_i)||_1$, N defines the number of samples in the training set and λ is a weighting factor.

B. MULTI-SCALE GAN ARCHITECTURE FOR IMAGE SUPER-RESOLUTION

One of the objectives of our work is to estimate a high resolution version with distinctive features of its low resolution input aerial image. The network is trained to learn a generating function G that aims to output photo-realistic images (according to a large distribution of images). Our basic deep generator network is illustrated in Fig. 1 which consists of B(=16) serially connected residual blocks with identical layout. Each residual block uses two convolution layers of 3×3 kernel and 64 feature maps followed by batch-normalization layers [42] and ParametricReLU [43] as the activation function. To increase the resolution of the input image, we employ two sub-pixel convolutional layers [44] in our generator network.

Although this architecture achieved promising results in recovering high-frequency information from low-resolution images; it cannot handle varying condition (sharpness, atmospheric turbulance, motion blur, etc.). Usually, the estimated super-resolved images suffer from image blurriness and shape distortions. Moreover, some details which are vital for producing natural looking images are missing in the super-resolved images.

One application of aerial image super-resolution is vehicle detection, which requires enough visual detail to distinguish vehicles from background (e.g., roads, buildings, trees, etc.) in super-resolved images. Our previous detection results [2] showed that this network is not able to produce a high-detection performance while performing on super-resolved images generated by the classical SRGAN. We follow the framework of Kazemi *et al.* [45] and Wang *et al.* [46] to build a progressive generator that learns to reconstruct a multi-stage network through a series of multi-scale image reconstructions. We train our generator model to produce multiple outputs at different resolutions as shown in Fig. 2. The main idea is to encourage the network to learn the image distribution at different scales. We enforce constraints on our network at two different image resolutions 256×256 and 512×512. When the network generates images of size 256×256, the first discriminator, $D1$ is pushing the generator to learn the probability distribution at that scale. Simultaneously, the second discriminator, $D2$ is contributing to help the generator to learn the distribution of the training images of size 512×512.

Gradually, the network learns to remove blurriness and recover missing object parts as it is trained at multi scales. Following this approach, it assures information transfer between images of different scales and generate more high-quality images.

We follow similar network structure for both discriminators $D1$ and $D2$. We adapt the architectural guidelines from Radford *et al.* [47] to design our discriminator. We utilize a LeakyReLU activation ($\alpha = 0.2$) and avoid max-pooling to

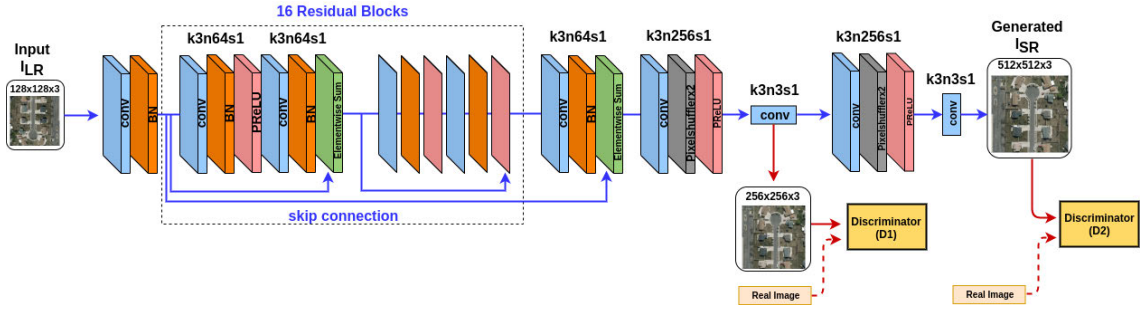

FIGURE 2. Architecture of multi-scale SRGAN (MsSRGAN) with corresponding kernel size (k), number of feature maps (n) and stride (s) indicated for each convolutional layer.

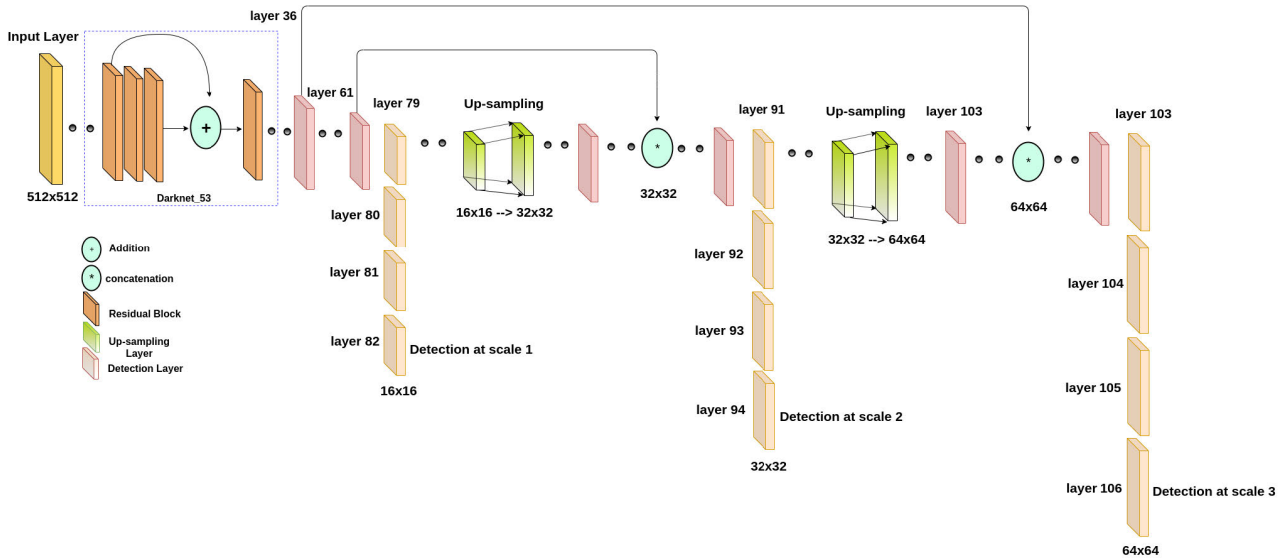

FIGURE 3. YOLOv3 architecture for vehicle detection at three scales showing residual block, upsampling layer as feature extractor.

ignore feature size reduction. Our discriminator has eleven convolutional layers, which use 4×4 filter kernels. Network employs strided convolutions to decrease image resolution while increasing the feature map size. At the end of the network, one dense layer and a final sigmoid activation function is added to obtain a probability for sample classification.

C. AERIAL VEHICLE DETECTION

Our goal is to perform vehicle detection on several aerial datasets. The datasets contain aerial vehicles of different sizes which require strong detection algorithm to extract contextual and semantic information of those target objects. In our research work, we use YOLOv3 of the state-of-the-art object detection algorithms to perform vehicle detection in real-time.

1) ARCHITECTURE DETAILS

The architecture of YOLOv3 shown in Fig. 3 is based on the idea of residual network which employs Darknet-53 convolutional network for feature extraction. To retrieve fine-grained information, it concatenates deeper layers with the earlier layers through up-sampling. YOLOv3 takes an image and divides it into $M \times M$ (16×16, 32×32 and 64×64 as in Fig. 3) grids. Then it applies classification and localization at each grid size. The grid cell is responsible for detecting object, if the center of the ground truth object falls within a grid cell. For each grid cell, a number of bounding boxes with their confidence scores and their associated class probabilities are generated using a fully convolutional network architecture. YOLOv3 performs multi-scale prediction applying the feature pyramid network (FPN) [48] concept. It predicts objects at three different scales of 16, 32 and 64 for large, medium and small object detection. YOLOv3 uses 9 anchor boxes while predicting objects. Design of the anchor boxes greatly impacts the performance of the detector. We have used k-means clustering to generate these anchors for each database. The final number of detection results by YOLOv3 is $M \times M \times (B * (4 + 1 + C))$. Here, $M \times M$ is the number of grid cells, B is predicted number of bounding boxes in a cell, 4 denotes the four coordinates of the bounding boxes and 1 is for the objectness score, C is the number of classes ($C = 1$:'vehicle' in our experiments). It uses

multi-label classification. Softmax is replaced by a logistic regression to compute objectness score. Instead of using mean squared error in calculating the classification loss, it uses the binary cross-entropy loss for each label.

D. OUR PROPOSED JOINT SUPER-RESOLUTION AND DETECTION NETWORK

In this paper, we propose an end-to-end multi-task model that jointly does super-resolution and vehicle detection in aerial imagery. Super-Resolution and vehicle detection for low-resolution aerial images have been considered as highly interrelated tasks. Usually, multi-task learning is adapted to address such highly correlated tasks as they can leverage significant information from each other. The vehicles in aerial scenes suffer from appearance ambiguity due to the low resolution characteristics of the images. In addition, it becomes challenging to deal with different sizes of vehicles with varying conditions such as blurry edges and lack of sharpness, etc. Moreover, the similarities between target vehicles and complex background make it even more difficult during detection.

In our previous work [2], super-resolution and vehicle detection networks were developed independently to help each other. We notice that the information extracted from the low-resolution space is not maximized when only one task is performed without utilizing the advantages of the other task (e.g., detection is performed on super-resolved images generated from already trained SR module). In other words, if we apply super-resolution and vehicle detection successively, it does not benefit from multi-tasking. Therefore, our goal is to create a bridge between these highly interrelated tasks so that they can get the maximum benefit from the multi-task learning. Hence, we propose the Joint-SRVDNet to generate distinctive super-resolved images with high perceptual quality and simultaneously locate vehicles on these super-resolved images. We have developed a MsGAN super-resolution module that explicitly incorporates the structural information (edges, sharpness, perceptual features defined by visual deterministic properties of objects) about targets into the super-resolution reconstruction process as well as jointly learns both the super-resolution and object detection modules together as presented in Fig. 4. As shown in Fig. 4 super-resolution and detection modules are cascaded to execute the joint training in an end-to-end fashion.

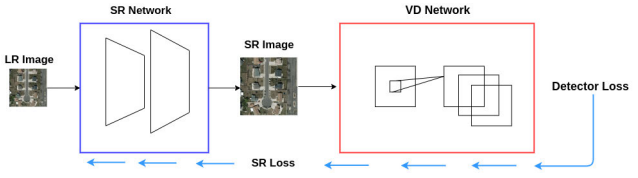

FIGURE 4. Architecture of our proposed model Joint-SRVDNet during the training process where the detector and super-resolution losses are back propagated to the generator.

The joint loss optimization of our model is difficult to converge from scratch compared to the training of each module independently. Therefore, we first train super-resolution module given the paired high-resolution and corresponding low-resolution aerial training images. Then we train detection module with high resolution images to obtain network parameters for further training. Finally, we fine tune both modules together and integrate into one unified framework by optimizing (7) where super-resolution and detection losses are jointly trained together. Such a training scheme leads to a better convergence. Our proposed network optimizes a combination of four different losses : adversarial loss, pixel-wise mean square error (MSE), perceptual loss, and detection loss. The adversarial loss aims to help generator to create solutions that are close to real images by differentiating between real and generated aerial images. The widely used pixel-wise MSE estimates an overly smoothed solution as it only measures pixel differences between super-resolved images and ground truth high resolution images. A perceptual loss using the pretrained VGG-19 network recovers photo-realistic textures, and a detection loss that aims for locating the target of interests with varying attributes such as lost edge details and structural features.

IV. LOSS FUNCTION

We combine multiple loss terms to train our proposed joint network. The ultimate final loss function includes pixel-wise MSE loss, perceptual loss, adversarial loss and detection loss.

A. PIXEL-WISE MSE LOSS

State-of-the-art image SR methods [12], [44] mostly rely on pixel-wise MSE loss to optimize the network. For the training images I_n^{HR} with their corresponding low-resolution I_n^{LR}, $n = 1,\ldots,N$, we can calculate the MSE loss also referred to as the content loss l_{cont} using the following equation:

$$L_{cont} = \frac{1}{N}\sum_{n=1}^{N}\frac{1}{WH}\sum_{x=1}^{W}\sum_{y=1}^{H}((I_n^{HR})_{x,y} - G(I_n^{LR})_{x,y})^2, \quad (3)$$

where W and H represent width and height of the image and $G(I_n^{LR})$ are the super-resolved images for N training samples.

Although MSE loss is the widely used optimization method for super-resolution which achieves high peak signal-to-noise ratios, the resulting estimates often lack fine texture details and are perceptually not convincing because of overly blurry results. In addition, MSE doesn't have ability to capture spatially varying high frequency information, as it is based on pixel-wise image differences.

B. PERCEPTUAL LOSS

Since optimizing the MSE loss is prone to overfitting when defined over the pixel-wise differences between estimated super-resolved images and ground truth high resolution images, Ledig *et al.* [6] propose the perceptual loss, which is defined as the MSE loss over high-level features extracted from the corresponding images. These features, which are extracted using a pretrained 19 layer VGG Network [49], map raw images to a lower dimensional and

representative subspace. Thus, optimizing the perceptual loss better preserves discriminative information and alleviate overfitting. The perceptual loss can be considered as the L2 distance between the feature representations of the generated super-resolved image and ground truth HR image. For N training samples we solve:

$$L_{per} = \frac{1}{N}\sum_{n=1}^{N}\frac{1}{C_jW_jH_j}\sum_{c=1}^{C_j}\sum_{x=1}^{W_j}\sum_{y=1}^{H_j} \times(\phi_j(I_n^{HR})_{c,x,y} - \phi_j(G(I_n^{LR}))_{c,x,y})^2, \quad (4)$$

where ϕ_j stands for feature map of j-th convolutional layer and C_j, W_j and H_j define the dimensions of the respective feature maps within the VGG19 network.

C. ADVERSARIAL LOSS

Since the network cannot learn to recover all high-frequency information by optimizing only the MSE or the perceptual losses, we also add the adversarial loss to the perceptual and the pixel-wise MSE losses to train our proposed network. The adversarial loss described by (1) pushes the solutions move towards the natural image manifold by training the generator to fool the discriminator by generating photo-realistic images, and training the discriminator to accurately classify "real" images from the generated ones (i.e., fake images). Thus, the estimated solutions reside on the real samples manifold. The adversarial loss l_{adv} defines the probability of the discriminator $D(G(I^{LR}))$ that the reconstructed image $G(I^{LR})$ is a real HR image. Both discriminators as shown in Fig. 2, use the following adversarial loss functions to optimize the network.

$$L_{adv} = \min_G \max_D [E_{I^{HR}\sim P_{train}(I^{HR})}[logD(I^{HR})] + E_{I^{LR}\sim P_G(I^{LR})}[log(1 - D(G(I^{LR})))]], \quad (5)$$

where $P_{train}(I^{HR})$ and $P_G(I^{LR})$ define the probability distribution of real high-resolution images and corresponding low-resolution images, respectively.

D. DETECTION LOSS

YOLOv3 is the combination of three losses: localization, confidence and classification loss. Equation (6) defines this loss. 1_{ij}^{obj} means the object is detected by j^{th} boundary box of grid cell i. x_i, y_i, w_i, h_i are the real ground truth bounding box coordinates whereas $\hat{x}_i$, $\hat{y}_i$, $\hat{w}_i$, $\hat{h}_i$ are the predicted bounding box coordinates. C_i is the box confidence score in cell i, $\hat{C}_i$ is the box confidence score for the predicted object:

$$L_{detection} = \lambda_{coord}\sum_{i=0}^{S^2}\sum_{j=0}^{B}1_{ij}^{obj}(x_i - \hat{x}_i)^2 + (y_i - \hat{y}_i)^2 + \lambda_{coord}\sum_{i=0}^{S^2}\sum_{j=0}^{B}1_{ij}^{obj}(\sqrt{w_i} - \sqrt{\hat{w}_i})^2 + (\sqrt{h_i} - \sqrt{\hat{h}_i})^2 + \sum_{i=0}^{S^2}\sum_{j=0}^{B}1_{ij}^{obj}l(C_i, \hat{C}_i) + \lambda_{noobj}\sum_{i=0}^{S^2}\sum_{j=0}^{B}1_{ij}^{noobj}l(C_i, \hat{C}_i) + \sum_{i=0}^{S^2}1_i^{obj}\sum_{c\in classes}l(p_i(c) - \hat{p}_i(c)). \quad (6)$$

E. JOINT LOSS OPTIMIZATION

Our proposed model can be viewed as a joint learning approach. The network is learning semantic information about targets from the training distribution so that the appearance of the target looks more clear and obvious in super-resolved images to help the detection module. In this section, we show how we combine the detection loss along with the pixel-wise MSE loss, perceptual loss and adversarial loss through an optimization to produce our desired output with full target details. Therefore, to show the dependency of different loss functions, lets assume W_{SR}, W_{VGG}, W_{dis} and W_d denote the parameter set for super-resolution model, pre-trained VGG 19 architecture, discriminator model and detection model, respectively. The parameterized version of the final loss function is as follows:

$$L = L_{cont}(I_n^{LR}; W_{SR}) + \alpha L_{per}(I_n^{LR}; W_{SR}, W_{VGG}) + \beta L_{adv}(I_n^{LR}; W_{SR}, W_{dis}) + \gamma L_{detection}(I_n^{LR}; W_{SR}, W_d). \quad (7)$$

We apply gradient descent algorithm to find the local minimum, and update the network's parameter by calculating the gradient $\nabla W = [\nabla W_{SR}\nabla W_d]$ with a learning rate η.

1) GRADIENT WITH RESPECT TO W_d

We calculate $\frac{\partial L}{\partial W_d}$ and use the standard back propagation algorithm as the following chain rule holds:

$$\frac{\partial L}{\partial W_d} = \sum_{n=1}^{N}\frac{\partial L}{\partial o_n}\frac{\partial o_n}{\partial W_d}, \quad (8)$$

where o_n defines a vector representation of the bounding box coordinates and confidence score. Again, $\frac{\partial L}{\partial o_n}$ involves three terms according to the definition as below:

$$\frac{\partial L}{\partial o_n} = \frac{\partial L_c}{\partial o_n} + \frac{\partial L_b}{\partial o_n} + \frac{\partial L_{conf}}{\partial o_n}, \quad (9)$$

where L_c, L_b simply calculate the loss for bounding box coordinates (e.g., center, width and height) and L_{conf} defines bounding box confidence score loss.

2) GRADIENT WITH RESPECT TO W_{SR}

To update the parameter set for SR model, we consider loss terms associated with the SR reconstruction process and apply gradient descent algorithm to find $\frac{\partial L}{\partial W_{SR}}$. The chain rule holds as follows:

$$\frac{\partial L}{\partial W_{SR}} = \sum_{n=1}^{N}\frac{\partial L}{\partial G(I_n^{LR})}\frac{\partial G(I_n^{LR})}{\partial W_{SR}}. \quad (10)$$

If we set the partial derivative of the loss function with respect to $G(I_n^{LR})$ and expand L, we get

$$\frac{\partial L}{\partial G(I_n^{LR})} = \frac{\partial L_{cont}}{\partial G(I_n^{LR})} + \alpha \frac{\partial L_{per}}{\partial G(I_n^{LR})} + \beta \frac{\partial L_{adv}}{\partial G(I_n^{LR})} + \gamma\left(\frac{\partial L_c}{\partial G(I_n^{LR})} + \frac{\partial L_b}{\partial G(I_n^{LR})} + \frac{\partial L_{conf}}{\partial G(I_n^{LR})}\right). \quad (11)$$

or, we can also express the above equation as follows:

$$\frac{\partial L}{\partial G(I_n^{LR})} = \frac{\partial L_{cont}}{\partial G(I_n^{LR})} + \alpha \frac{\partial L_{per}}{\partial G(I_n^{LR})} + \beta \frac{\partial L_{adv}}{\partial G(I_n^{LR})} + \gamma \frac{\partial L_{detection}}{\partial G(I_n^{LR})}. \quad (12)$$

We can summarize the optimization steps in Algorithm 1.

Algorithm 1 Our Proposed Joint-SRVDNet Model Training

Input: Training samples, $I = < I_n^{LR}, I_n^{HR} >$
Ensure: Model parameters set $W = [W_{SR}, W_d]$
while not converged **do**
t=t+1;
calculate the partial derivative $\frac{\partial L}{\partial W_d}$;
calculate the partial derivative $\frac{\partial L}{\partial o_n}$;
execute back propagation from top layer to the bottom layer of detection to obtain $\frac{\partial L}{\partial W_d}$;
calculate the partial derivative $\frac{\partial L}{\partial G(I_n^{LR})}$;
add the $\frac{\partial L_{cont}}{\partial G(I_n^{LR})}$, $\frac{\partial L_{per}}{\partial G(I_n^{LR})}$ and $\frac{\partial L_{adv}}{\partial G(I_n^{LR})}$ to the derivative $\frac{\partial L}{\partial G(I_n^{LR})}$ obtained in step 6;
execute back propagation from the last layer to the first layer of SR to obtain $\frac{\partial L}{\partial W_{SR}}$;
update the parameter W by $W^{t+1} = W^t + \eta \nabla W$;

V. TRAINING DETAILS

A. EXPERIMENTAL DATA

We evaluate the performance of our proposed method on three publicly available benchmark datasets: Vehicle Detection in Aerial Imagery (VEDAI) dataset [38], xView dataset [40] and DOTA dataset [39]. In this section, detailed description of the training datasets are provided. Then, we describe the implementation and experimental strategies.

1) VEHICLE DETECTION IN AERIAL IMAGERY (VEDAI) DATASET

The VEDAI dataset is a publicly available benchmark for small target recognition especially vehicle detection in aerial images. This dataset has around 1,210 images of two different resolutions such as $1,024 \times 1,024$ pixels and 512×512 pixels. The images mostly contain small vehicles having diverse backgrounds, multiple orientations, lighting/shadowing changes, specularities or occlusions. In addition, it includes nine different classes of vehicles, namely the plane, boat, camping car, car, pick-up, tractor, truck, van, and the other category. We consider all classes as a single class namely 'vehicle' for our task. For training and testing, we split the dataset into 1,100 and 271 images, respectively. The number of samples in our dataset is small for analyzing the proposed network. Therefore, to make the model more robust to different features, we have used different augmentation techniques such as image sharpening and flipping.

2) DATASET FOR OBJECT DETECTION IN AERIAL IMAGES (DOTA)

DOTA is a large-scale multi-sensor and multi-resolution aerial dataset. This dataset is challenging because of its immense number of object instances from various categories exhibiting a wide variety of scales, orientations and shapes. The dataset contains 2,806 images of varying size ranging from 800×800 to $4,000 \times 4,000$ pixels. We have created patches of size 512×512 from the original images. The complex aerial scenes present in this dataset are collected from Google Earth, satellite JL-1 and satellite GF-2. The dataset has fifteen categories of objects namely plane, ship, storage tank, swimming pool, ground track field, harbor, bridge, large vehicle, small vehicle, helicopter, roundabout, soccer ball field, basketball court, baseball diamond and tennis court. We have omitted class swimming pool, ground track field, harbor, bridge, roundabout, soccer ball field, basketball court, baseball diamond and tennis court and unified the remaining six classes as one class 'vehicle'.

3) X-VIEW DATASET

xView is currently the largest publicly available dataset collected from WorldView-3 satellites. The dataset contains 60 highly imbalanced classes. To overcome the problem of poor detection performance, we have generalized all the classes into one class 'vehicle'. It contains around 1 million objects covering 1,400 km^2 of the earth surface. The dataset is cropped into smaller patches of 512×512. Each pixel corresponds to $0.3 \times 0.3 m^2$ area in the ground. The annotation provided is in geoJSON format and contains information about the bounding boxes for objects present in an image.

B. IMPLEMENTATION STRATEGIES AND TRAINING PARAMETERS

At the beginning, we separately train both sub-networks: super-resolution and detection modules to obtain their network weights which have been used to initialized the joint network of our proposed model. We perform all experiments using 4x upsampling factor between low- and high-resolution images. To obtain LR images, bicubic kernel is used to downscale the HR images with a scale factor of 4. During implementation, we use input images of size 128×128 to super-resolve to 512×512.

To train a deep neural network using a small dataset is troublesome due to the over-fitting problem. One approach to overcome this difficulty is to use data augmentation, specifically sharpening and [horizontal, veritical] flipping.

TABLE 1. Comparison of super-resolution architectures for upscale factor 4x on aerial datasets.

Dataset	VEDAI-VISIBLE				VEDAI-IR				XVIEW				DOTA			
Algorithm	PSNR	MSSIM	UQI	VIF	PSNR	MSSIM	UQI	VIF	PSNR	MSSIM	UQI	VIF	PSNR	MSSIM	UQI	VIF
Bicubic	22.060	0.912	0.945	0.560	22.513	0.920	0.980	0.597	15.856	0.419	0.663	0.416	24.617	0.936	0.963	0.349
SRGAN	25.856	0.918	0.981	0.607	25.876	0.928	0.988	0.627	17.799	0.517	0.783	0.515	24.893	0.941	0.959	0.514
MsSRGAN	26.899	0.927	0.991	0.653	27.890	0.939	0.995	0.683	18.838	0.541	0.794	0.550	28.474	0.975	0.971	0.623
DenseNet GAN	29.9				-				-				-			
Joint-SRVDNet (Ours)	**30.338**	**0.969**	**0.995**	**0.693**	**29.227**	**0.958**	**0.999**	**0.713**	**20.550**	**0.617**	**0.795**	**0.562**	**31.360**	**0.987**	**0.975**	**0.712**

For the super-resolution network, we adapt the Adam optimizer with a momentum of 0.9 and a batch size of 4. We initially set the learning rate at 10^{-4} which decays by a factor of 0.1 after every 5 epochs. For YOLOv3 model, we optimize the network by Adam with a learning rate of 10^{-4} and 10^{-6} with batch size 16. For non-maximum suppression, the threshold is set to 0.5. Following (6), the network calculates bounding box loss, coordinate loss, class confidence scores and objectness score for each detection layer. These losses are offset to predict the object probability, class probability and bounding box coordinates for each grid which together represents an object at that grid. Usually the network generates several bounding boxes and selects the bounding box with the highest Intersection over Union (IoU). For each aerial dataset, we train both networks for 10 epochs and achieve satisfactory results.

For joint-training, we consider the sub-networks together and train it as a unified network. To initialize the overall network, we employ the weights from the independently pre-trained models. We choose Adam as the optimizer by setting initial learning rate as 10^{-4}. The learning rate decays exponentially with moving average decay of 0.9991. After training for 4 epochs with a mini-batch size 1, we observe significant improvement in results which verifies that our proposed method has been successfully implemented. We implement the proposed network using tensorflow framework and train it over two NVIDIA Titan XpGPU. Moreover, we explored the effect of varying the hyperparameters (α, β and γ) adapted in (7) to further validate the results of our model. The analysis of the hyperparameters has been made on the test dataset and their impact will be discussed in the ablation study.

VI. EXPERIMENTAL RESULTS ANALYSIS

In this section, we present comparative results for both image super-resolution and vehicle detection on several aerial datasets to evaluate the performance of our proposed model. We compare the reconstruction quality of the super-resolved images generated by our proposed network to other methods including bicubic interpolation, SRGAN [6], MsSRGAN [45] and DenseNet GAN [50] on overhead datasets which were described in the previous section. Then we investigate vehicle detection performance of our network in terms of mean Average Precision (mAP) and F1 score. For more comprehensive performance analysis, we provide precision-recall curve and plot true positive rate (TPR) against false positive rate (FPR).

A. SUPER-RESOLUTION RESULTS

We have reported the super-resolution results of our experiments using several objective image quality metrics such as Peak Signal-to-Noise ratio (PSNR), Multi-scale Structural Similarity (MSSIM) [57], Universal image Quality Index (UQI) [58] and Visual Information Fidelity (VIF) [59] on a validation subset of images for each dataset. Table 1 shows a comparative analysis of our approach with other GAN based state-of-the-art techniques. For comparison, first we include results from bicubic interpolation method. Then we follow SRGAN architecture; one of the pioneering works on super-resolution using GAN introduced by Ledig et al [6]. As expected, the performance of this network is much better than the previous approaches due to addition of the perceptual loss which enables the network to produce images with sharper edges and features. After that, we notice, adding multiple intermediatory discriminators to the same generator architecture as the SRGAN helps to generate even higher quality images with more perceptual similarity which often lacks in the generated images from the SRGAN. We refer to this network as MsSRGAN which is actually introduced in [45] to handle super-resolution for facial images. We utilize this concept and conduct experimients on aerial datasets. We observe slight improvements in the reconstructed SR results and report it for comparison. Moreover, we have also compared our results with DenseNet GAN [50] for VEDAI dataset. All these GAN based methods use perceptual loss, MSE loss along with adversarial loss even if they modify their architecture which shows gradual improvement in their solutions. However, they cannot meet the demand of current situation. They are often unable to extract fine texture details of the targets (vehicle) of interest. So, our aim is to produce solutions which contain clear view of our targets with fine-grained details. We design a loss function which incorporates detecton loss along with other losses (perceptual loss, adversarial loss and MSE loss) which helps to reach our goal. Table 1 shows that our proposed algorithm obtains the highest PSNR, MSSIM, UQI and VIF scores which proves the quantitative effectiveness of our proposed network. To show the quality of the super-resolved images specifically for the target regions produced by our network, we select a small area around the targets and show the gradual progression of different SR results which are visible in Fig. 5. We have conducted our experiments for 4x enhancement (128×128 to 512×512). We can see that in the super-resolved image the selected area around the target and the target itself is getting more

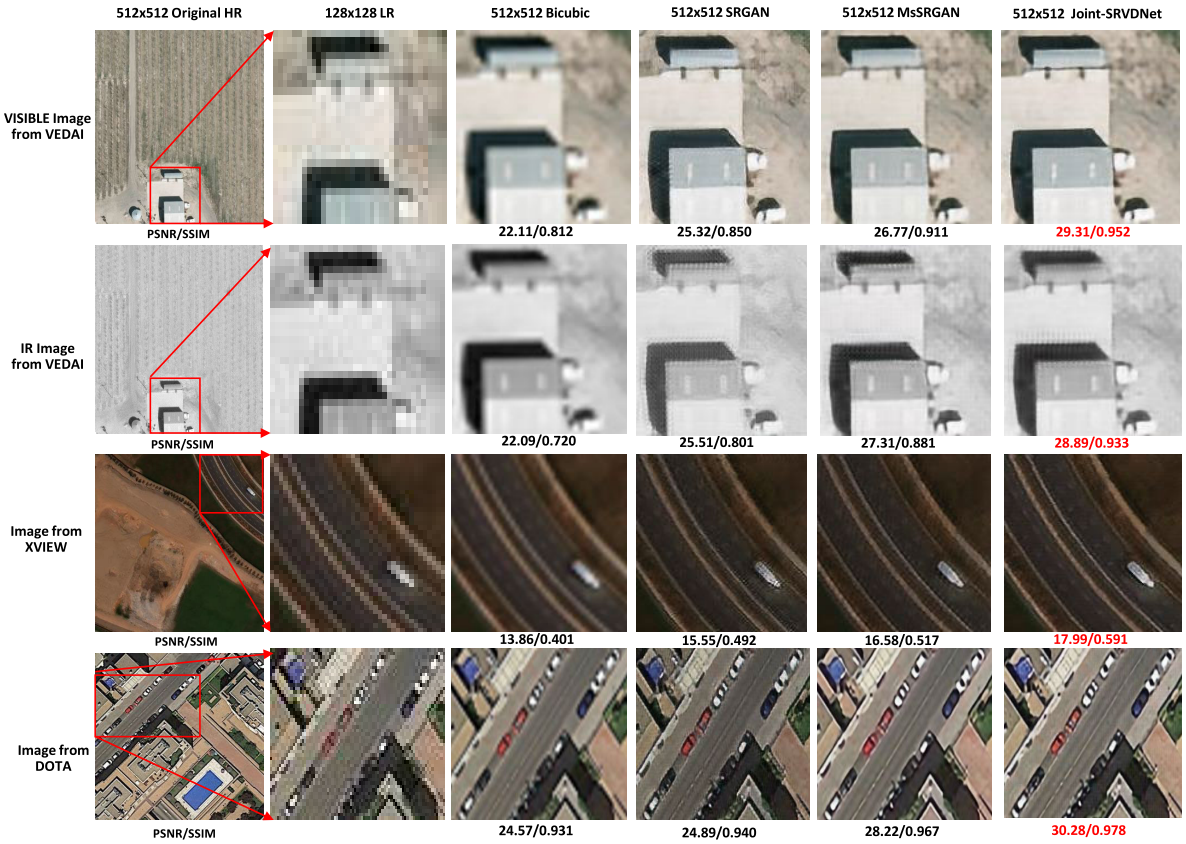

FIGURE 5. Visual results using Bicubic, SRGAN, MsSRGAN and our proposed model Joint-SRVDNet with scaling factor 4 over VEDAI, xView and DOTA datasets.

TABLE 2. Comparative detection performance in terms of mean average precision (mAP) and F1-score of the proposed network and existing state-of-the-art approaches. Red bold indicates the optimal performance using actual HR imagery and blue bold indicates the second optimal performance using SR images generated by our proposed network.

Dataset	VEDAI-VISIBLE		VEDAI-IR		XVIEW		DOTA	
Architectures	mAP@0.5	F1 score	mAP@0.5	F1 score	mAP@0.5	F1 score	mAP@0.5	F1 score
Ren, et al. (Z&F) [51]	32.00	0.212	-		-		-	
Girshik, et al. (VGG-16) [52]	37.30	0.224	-		-		-	
Ren, et al. (VGG-16) [51]	40.90	0.225	-		-		-	
Zhong, et al. [53]	50.20	0.305	-		-		-	
Chen, et al. [54]	59.50	0.451	-		-		-	
YOLOv3_SRGAN_512	62.45	0.591	70.10	0.687	53.47	0.479	86.18	0.837
YOLOv3_MsSRGAN_512	66.74	0.643	74.61	0.723	57.96	0.494	87.02	0.859
YOLOv3_SSSDet_512 [55]	45.97		-		-		79.52	
Ju, et al. [56]	-		-		-		88.63	
YOLOv3_Joint-SRVDNet_512 (Ours)	**72.46**	**0.702**	**80.40**	**0.792**	**61.50**	**0.671**	**90.01**	**0.893**
YOLOv3_HR_512	**85.33**	**0.826**	**85.66**	**0.876**	**66.02**	**0.687**	**94.56**	**0.933**

close to the original one as bicubic interpolation, SRGAN, MsSRGAN and our network have been applied successively. Visual results are showing that recovering high frequency details in low-resolution domain is extremely difficult but it is captured by using our proposed network. The ultimate goal of our work is to recover target details which has a great effect on the detection performance.

B. DETECTION PERFORMANCE ANALYSIS

Table 2 summarizes a comparative performance measures of our proposed model and other leading state-of-the-art algorithms in terms of mAP and F1 score for aerial vehicle detection. The mAP values and F1 scores are reported on VEDAI, xView and DOTA datsets for most of the algorithms based on the availability. We calculate the mAP as the average of the maximum precisions at different recall values in the range (0.0 $\sim$ 1.0). For each dataset, we show the precision-recall graphs at different IoU thresholds (0.3 $\sim$ 0.7) for YOLOv3 performed on super-resolved images generated from SRGAN, MsSRGAN and our proposed network as shown in Fig. 6. We have evaluated all the methods over the same set of test data. we can conclude that our proposed technique is much more stable and robust for aerial vehicle detection in comparison to the current

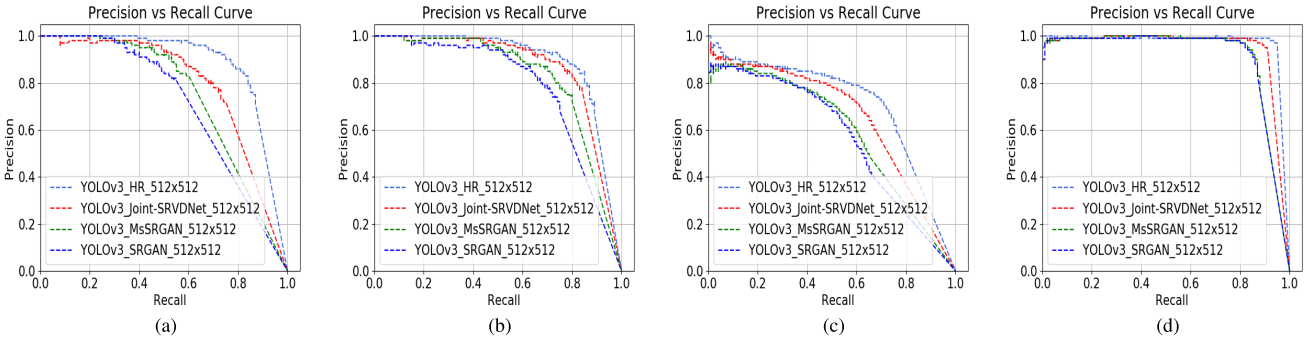

FIGURE 6. Precision-recall graph of the state-of-the-art object detector YOLOv3 performed on the original 512 × 512 high-resolution test images and the corresponding super-resolved images generated from SRGAN, MsSRGAN and our proposed Joint-SRVDNet over (a) VEDAI-VISIBLE, (b) VEDAI-IR, (c) xView and (d) DOTA.

state-of-the-art detection techniques. Besides, we include detection results of recent CNN-based detectors: Faster R-CNN [51] with Z&F model, Faster R-CNN [51] with VGG-16 model and Fast R-CNN [52] with VGG-16 model for VEDAI dataset. Also, we have compared our detection performance with [53] and most recently proposed detection algorithm [54]. It is easily noticeable from the results presented in Table 2 that our proposed model demonstrates the best performance compared to these detection methods and yields the 2nd best mAP (72.46%) and F1-Score (0.702) for VEDAI. For comparison with the current DCNN based approaches, we include the results of SSSDet [55] reported in their publications for VEDAI and DOTA as they claim to achieve the most competitive results on such datasets. We observe that detection performance of our method on VEDAI and DOTA datasets is extremely good compared to [55] in terms of mAP. As shown in Table 2, the performance of our proposed scheme is 26.49% and 10.49% higher than [55] for VEDAI-VISIBLE and DOTA datasets respectively.

Again, compared with the detection performance of super-resolved images generated from the existing most resent MsSRGAN based SR architecture, our method has achieved almost 5.75% higher mAP and 7% better F1 score for both VEDAI-VISIBLE and VEDAI-IR images. Moreover, for both dataset, we observe that the detection performance of our network (indicated by blue bold in Table 2) is also close to the optimal performance of the detector using original HR imagery, which is shown at the bottom row of Table 2. We also report mAP and F1 score for the xView satellite images which is very challenging as it contains extremely small targets in the image. Due to the low-resolution, targets do not contain detailed information which might help the detection task. As a result we cannot achieve satisfactory performance like other two datasets. However, still we have achieved 3.54% higher mAP and 2% better F1 score than the performance of super-resolved images from MsSRGAN and it is also close to the detection performance of the original 512 × 512 high resolution images. We also investigate our model's performance on DOTA dataset. During experiments, we notice a great improvement in detection performance for this dataset as shown in Fig. 6(d) and fourth column of Table 2. The targets in this dataset seem to have the best appearance quality among two other datasets which has contributed to secure high detection performance. Therefore, we obtain promising results compared to [60] as well as for all the other algorithms.

In addition, Fig. 6 helps to analysis the relationship between precision and recall rate for all datasets. It is obvious from the precision-recall plots that, our method (YOLOv3_Joint-SRVDNet_512 × 512 in red curve) is significantly better than the other GAN based methods (YOLOv3_MsSRGAN_512 × 512 in green curve and YOLOv3_SRGAN_512×512 in blue curve) and more specifically, the performance gain is comparable to the detection performance of the original 512 × 512 high resolution images.

However, some important information might be missing if we only depend on precision-recall metric and F1 scores to determine the performance of our proposed method. For more robust analysis, we focus on plotting receiver operating characteristic curve (ROC) to study the characteristics of detection results. ROC curve can be drawn by plotting TPR against FPR at different thresholds. ROC curve reflects the relationship between TPR and FPR which may help to compare our method to other detection approaches. To show the comparative detection results for all datasets similar to Fig. 6, we have plotted ROC curves for different detection methods in Fig. 7. Furthermore, we calculate the area under the ROC curve known as AUC which can be considered as another important metric to evaluate detection accuracy. According to the analysis of detection results of different frameworks in terms of AUC, the performance of our proposed system is 6.2%, 4.2%, 5.5% and 2.8% higher in comparison to detection performance of super-resolved images generated from MsSRGAN over VEDAI-VISIBLE, VEDAI-IR, xView and DOTA dataset, respectively.

VII. ABLATION STUDY

To achieve the best version of our proposed model, we made several experiments through changing the value of

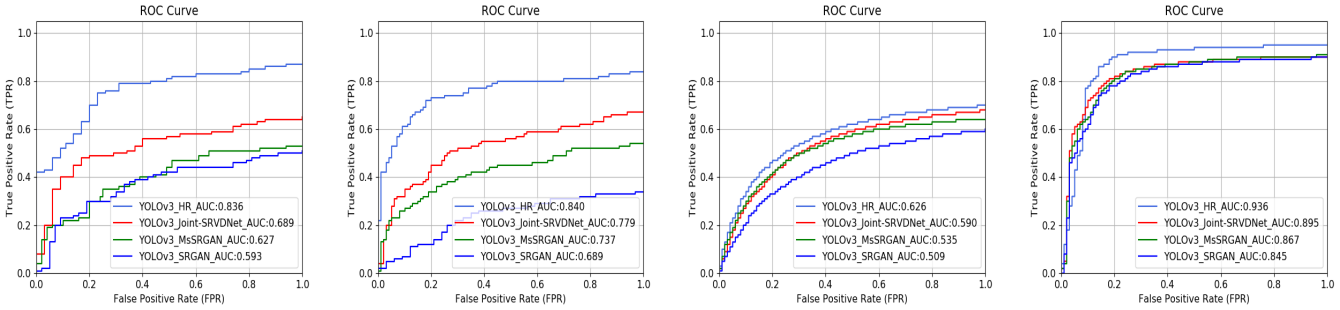

FIGURE 7. ROC curves showing true-positive versus false-positive rates of the YOLOv3 object detector performed on the original 512 × 512 high-resolution test images and the corresponding super-resolved images generated from SRGAN, MsSRGAN and our proposed Joint-SRVDNet over (a) VEDAI-VISIBLE, (b) VEDAI-IR, (c) xView and (d) DOTA.

TABLE 3. Super-resolution results of our proposed model using different hyperparameter settings for upscale factor 4x on the aerial test datasets. Magenta bold indicates the optimal SR results generated by our proposed network.

Dataset	VEDAI-VISIBLE				VEDAI-IR				XVIEW				DOTA			
Hyperparameter Settings	PSNR	MSSIM	UQI	VIF	PSNR	MSSIM	UQI	VIF	PSNR	MSSIM	UQI	VIF	PSNR	MSSIM	UQI	VIF
$\alpha=2\times10^{-6}, \beta=10^{-2}, \gamma=10^{-2}$	27.060	0.812	0.745	0.690	26.513	0.720	0.780	0.697	17.856	0.529	0.523	0.436	24.327	0.845	0.813	0.457
$\alpha=\mathbf{2\times10^{-6}}, \beta=\mathbf{10^{-3}}, \gamma=\mathbf{10^{-3}}$	**30.338**	**0.969**	**0.995**	**0.693**	**29.227**	**0.958**	**0.999**	**0.713**	**20.550**	**0.617**	**0.795**	**0.562**	**31.360**	**0.987**	**0.975**	**0.712**
$\alpha=2\times10^{-6}, \beta=10^{-2}, \gamma=10^{-4}$	26.746	0.723	0.716	0.705	25.976	0.723	0.789	0.778	16.799	0.427	0.654	0.515	24.212	0.841	0.849	0.524

TABLE 4. Vehicle detection results in terms of mean average precision (mAP) and F1-score of our proposed model using different hyperparameter settings on the aerial test datasets. Cyan bold indicates the second optimal performance using SR images generated by our proposed network.

Dataset	VEDAI-VISIBLE		VEDAI-IR		XVIEW		DOTA	
Hyperparameters Settings	mAP@0.5	F1 score	mAP@0.5	F1 score	mAP@0.5	F1 score	mAP@0.5	F1 score
$\alpha=2\times10^{-6}, \beta=10^{-2}, \gamma=10^{-2}$	68.89	0.678	77.78	0.756	59.61	0.556	88.59	0.778
$\alpha=\mathbf{2\times10^{-6}}, \beta=\mathbf{10^{-3}}, \gamma=\mathbf{10^{-3}}$	**72.46**	**0.702**	**80.40**	**0.792**	**61.50**	**0.671**	**90.01**	**0.893**
$\alpha=2\times10^{-6}, \beta=10^{-2}, \gamma=10^{-4}$	69.90	0.685	78.79	0.771	58.88	0.521	89.12	0.789

hyperparameters to see the impact of the hyperparameter changes on the original version of our work. We have summarized the analysis in Table 3 and 4.

A. HYPERPARAMETER ANALYSIS

We analyze the values of α, β and γ adapted in (7) in order to obtain better quantitative results in aerial datasets. In (7), we have used α, β and γ as weight factors to numerically balance the magnitude of different losses which accelerates the total loss convergence. The network can benefit from the relative influence of different loss functions, which is somehow guided by the weight factors. Since there is no rule of choosing the optimum parameters for the model, we conduct a series of experiments to find out the optimal parameters of the proposed model. We observe that the optimal values lead the training to generate real-looking images with full target details (edges, sharpness, perceptual features, etc.), that has been already reported in the experimental result analysis section. In Table 3 and 4, we show the average accuracy of our model varying these hyperparameters on several aerial test datasets.

Among the above settings, we report the results for the second setting (indicated by bold Magenta, Cyan) in Table 1, Table 2, and Fig 5, Fig 6, and Fig 7 as it provides the best results that is almost comparable to the original HR.

VIII. CONCLUSION

To address the challenge of detecting small targets (vehicles) in aerial images, we propose an approach that jointly optimizes super-resolution and detection modules. The purpose of our algorithm is to generate high quality super-resolved images from lower-resolution images, so that larger areas can be surveilled with minimal degradation in detection performance. With extensive experiments we demonstrated that our proposed joint network is able to learn and extract features from low-resolution domain which reflects in the generated super-resolved images produced by the network and helps to improve detection performance. Most importantly, the proposed network has two vital contributions: for super-resolution task, using multi-scale GAN approach instead of classical SRGAN approach makes the detection task easier by adding more details in the super-resolved images which is essential to locate objects in the aerial images. Second, network's total loss integrates detection loss during super-resolution training which helps the SR module to specially learn the target area so that those specific area gets more obvious in the final super-resolution results. To evaluate our model's performance we conduct experiments on several publicly available datasets and the results indicate that compared with the leading state-of-the-art super-resolution and detection approaches, our proposed network achieves

impressive results and it may have great impact on remote sensing community.

REFERENCES

[1] S. Cao, Y. Yu, H. Guan, D. Peng, and W. Yan, "Affine-function transformation-based object matching for vehicle detection from unmanned aerial vehicle imagery," *Remote Sens.*, vol. 11, no. 14, p. 1708, 2019.

[2] S. N. Ferdous, M. Mostofa, and N. Nasrabadi, "Super resolution-assisted deep aerial vehicle detection," in *Proc. Artif. Intell. Mach. Learn. for Multi-Domain Operations Appl.*, May 2019, Art. no. 1100617.

[3] T. Aspiras, R. Liu, and V. K. Asari, "Convolutional auto-encoder for vehicle detection in aerial imagery (conference presentation)," in *Proc. Pattern Recognit. Tracking XXX*, vol. 10995, May 2019, Art. no. 109950.

[4] M. Y. Yang, W. Liao, X. Li, Y. Cao, and B. Rosenhahn, "Vehicle detection in aerial images," *Photogramm. Eng. Remote Sens.*, vol. 85, no. 4, pp. 297–304, 2019.

[5] I. Goodfellow, J. Pouget-Abadie, M. Mirza, B. Xu, D. Warde-Farley, S. Ozair, A. Courville, and Y. Bengio, "Generative adversarial nets," in *Proc. Adv. Neural Inf. Process. Syst.*, 2014, pp. 2672–2680.

[6] C. Ledig, L. Theis, F. Huszar, J. Caballero, A. Cunningham, A. Acosta, A. Aitken, A. Tejani, J. Totz, Z. Wang, and W. Shi, "Photo-realistic single image super-resolution using a generative adversarial network," in *Proc. IEEE Conf. Comput. Vis. Pattern Recognit.*, Jul. 2017, pp. 4681–4690.

[7] J. Hoffman, E. Tzeng, T. Park, J.-Y. Zhu, P. Isola, K. Saenko, A. A. Efros, and T. Darrell, "CyCADA: Cycle-consistent adversarial domain adaptation," 2017, *arXiv:1711.03213*. [Online]. Available: http://arxiv.org/abs/1711.03213

[8] J. Shermeyer and A. Van Etten, "The effects of super-resolution on object detection performance in satellite imagery," in *Proc. IEEE Conf. Comput. Vis. Pattern Recognit. Workshops*, Jun. 2019.

[9] C. C. Borel-Donohue and S. S. Young, "Image quality and super resolution effects on object recognition using deep neural networks," in *Proc. Artif. Intell. Mach. Learn. Multi-Domain Operations Appl.*, vol. 11006, May 2019, Art. no. 110061.

[10] J. Redmon, S. Divvala, R. Girshick, and A. Farhadi, "You only look once: Unified, real-time object detection," in *Proc. IEEE Conf. Comput. Vis. Pattern Recognit.*, Jun. 2016, pp. 779–788.

[11] J. Redmon and A. Farhadi, "YOLOv3: An incremental improvement," 2018, *arXiv:1804.02767*. [Online]. Available: http://arxiv.org/abs/1804.02767

[12] C. Dong, C. C. Loy, K. He, and X. Tang, "Image super-resolution using deep convolutional networks," *IEEE Trans. Pattern Anal. Mach. Intell.*, vol. 38, no. 2, pp. 295–307, Feb. 2016.

[13] J. Kim, J. K. Lee, and K. M. Lee, "Accurate image super-resolution using very deep convolutional networks," in *Proc. IEEE Conf. Comput. Vis. Pattern Recognit.*, Jun. 2016, pp. 1646–1654.

[14] J. Kim, J. K. Lee, and K. M. Lee, "Deeply-recursive convolutional network for image super-resolution," in *Proc. IEEE Conf. Comput. Vis. Pattern Recognit.*, Jun. 2016, pp. 1637–1645.

[15] K. He, X. Zhang, S. Ren, and J. Sun, "Deep residual learning for image recognition," in *Proc. IEEE Conf. Comput. Vis. Pattern Recognit.*, Jun. 2016, pp. 770–778.

[16] D. Eigen, J. Rolfe, R. Fergus, and Y. LeCun, "Understanding deep architectures using a recursive convolutional network," 2013, *arXiv:1312.1847*. [Online]. Available: http://arxiv.org/abs/1312.1847

[17] M. Liang and X. Hu, "Recurrent convolutional neural network for object recognition," in *Proc. IEEE Conf. Comput. Vis. Pattern Recognit.*, Jun. 2015, pp. 3367–3375.

[18] R. Socher, B. Huval, B. Bath, C. D. Manning, and A. Y. Ng, "Convolutional-recursive deep learning for 3D object classification," in *Proc. Adv. Neural Inf. Process. Syst.*, 2012, pp. 656–664.

[19] J. Bruna, P. Sprechmann, and Y. LeCun, "Super-resolution with deep convolutional sufficient statistics," 2015, *arXiv:1511.05666*. [Online]. Available: http://arxiv.org/abs/1511.05666

[20] L. Gatys, A. S. Ecker, and M. Bethge, "Texture synthesis using convolutional neural networks," in *Proc. Adv. Neural Inf. Process. Syst.*, 2015, pp. 262–270.

[21] J. Johnson, A. Alahi, and L. Fei-Fei, "Perceptual losses for real-time style transfer and super-resolution," in *Proc. Eur. Conf. Comput. Vis.* Cham, Switzerland: Springer, 2016, pp. 694–711.

[22] H. Zhang, T. Xu, H. Li, S. Zhang, X. Wang, X. Huang, and D. Metaxas, "StackGAN: Text to photo-realistic image synthesis with stacked generative adversarial networks," in *Proc. IEEE Int. Conf. Comput. Vis.*, Oct. 2017, pp. 5907–5915.

[23] T. Zhao and R. Nevatia, "Car detection in low resolution aerial images," *Image Vis. Comput.*, vol. 21, no. 8, pp. 693–703, Aug. 2003.

[24] J.-Y. Choi and Y.-K. Yang, "Vehicle detection from aerial images using local shape information," in *Proc. Pacific-Rim Symp. Image Video Technol.* Cham, Switzerland: Springer, 2009, pp. 227–236.

[25] H.-Y. Cheng, C.-C. Weng, and Y.-Y. Chen, "Vehicle detection in aerial surveillance using dynamic Bayesian networks," *IEEE Trans. Image Process.*, vol. 21, no. 4, pp. 2152–2159, Apr. 2012.

[26] J. Carlet and B. Abayowa, "Fast vehicle detection in aerial imagery," 2017, *arXiv:1709.08666*. [Online]. Available: http://arxiv.org/abs/1709.08666

[27] J. Sang, Z. Wu, P. Guo, H. Hu, H. Xiang, Q. Zhang, and B. Cai, "An improved YOLOv2 for vehicle detection," *Sensors*, vol. 18, no. 12, p. 4272, 2018.

[28] J. Ogier du Terrail and F. Jurie, "Faster RER-CNN: Application to the detection of vehicles in aerial images," 2018, *arXiv:1809.07628*. [Online]. Available: http://arxiv.org/abs/1809.07628

[29] A. Soleimani, N. M. Nasrabadi, E. Griffith, J. Ralph, and S. Maskell, "Convolutional neural networks for aerial vehicle detection and recognition," in *Proc. IEEE Nat. Aerosp. Electron. Conf. (NAECON)*, Jul. 2018, pp. 186–191.

[30] M. Ying Yang, W. Liao, X. Li, and B. Rosenhahn, "Vehicle detection in aerial images," 2018, *arXiv:1801.07339*. [Online]. Available: http://arxiv.org/abs/1801.07339

[31] Z. Deng, X. Hu, L. Zhu, X. Xu, J. Qin, G. Han, and P.-A. Heng, "R^3net: Recurrent residual refinement network for saliency detection," in *Proc. 27th Int. Joint Conf. Artif. Intell.*, Jul. 2018, pp. 684–690.

[32] M. Haris, G. Shakhnarovich, and N. Ukita, "Task-driven super resolution: Object detection in low-resolution images," 2018, *arXiv:1803.11316*. [Online]. Available: http://arxiv.org/abs/1803.11316

[33] E. Ataer-Cansizoglu, M. Jones, Z. Zhang, and A. Sullivan, "Verification of very low-resolution faces using an identity-preserving deep face super-resolution network," 2019, *arXiv:1903.10974*. [Online]. Available: http://arxiv.org/abs/1903.10974

[34] J. Wu, S. Ding, W. Xu, and H. Chao, "Deep joint face hallucination and recognition," 2016, *arXiv:1611.08091*. [Online]. Available: http://arxiv.org/abs/1611.08091

[35] Y. Pang, J. Cao, J. Wang, and J. Han, "JCS-net: Joint classification and super-resolution network for small-scale pedestrian detection in surveillance images," *IEEE Trans. Inf. Forensics Security*, vol. 14, no. 12, pp. 3322–3331, Dec. 2019.

[36] P. Dollar, C. Wojek, B. Schiele, and P. Perona, "Pedestrian detection: A benchmark," in *Proc. IEEE Conf. Comput. Vis. Pattern Recognit.*, Jun. 2009, pp. 304–311.

[37] A. Geiger, P. Lenz, and R. Urtasun, "Are we ready for autonomous driving? The KITTI vision benchmark suite," in *Proc. IEEE Conf. Comput. Vis. Pattern Recognit.*, Jun. 2012, pp. 3354–3361.

[38] S. Razakarivony and F. Jurie, "Vehicle detection in aerial imagery: A small target detection benchmark," *J. Vis. Commun. Image Represent.*, vol. 34, pp. 187–203, Jan. 2016.

[39] G.-S. Xia, X. Bai, J. Ding, Z. Zhu, S. Belongie, J. Luo, M. Datcu, M. Pelillo, and L. Zhang, "DOTA: A large-scale dataset for object detection in aerial images," in *Proc. IEEE/CVF Conf. Comput. Vis. Pattern Recognit.*, Jun. 2018, pp. 3974–3983.

[40] D. Lam, R. Kuzma, K. McGee, S. Dooley, M. Laielli, M. Klaric, Y. Bulatov, and B. McCord, "XView: Objects in context in overhead imagery," 2018, *arXiv:1802.07856*. [Online]. Available: http://arxiv.org/abs/1802.07856

[41] P. Isola, J.-Y. Zhu, T. Zhou, and A. A. Efros, "Image-to-Image translation with conditional adversarial networks," in *Proc. IEEE Conf. Comput. Vis. Pattern Recognit.*, Jul. 2017, pp. 1125–1134.

[42] S. Ioffe and C. Szegedy, "Batch normalization: Accelerating deep network training by reducing internal covariate shift," 2015, *arXiv:1502.03167*. [Online]. Available: http://arxiv.org/abs/1502.03167

[43] K. He, X. Zhang, S. Ren, and J. Sun, "Delving deep into rectifiers: Surpassing human-level performance on ImageNet classification," in *Proc. IEEE Int. Conf. Comput. Vis.*, Dec. 2015, pp. 1026–1034.

[44] W. Shi, J. Caballero, F. Huszár, J. Totz, A. P. Aitken, R. Bishop, D. Rueckert, and Z. Wang, "Real-time single image and video super-resolution using an efficient sub-pixel convolutional neural network," in *Proc. IEEE Conf. Comput. Vis. Pattern Recognit.*, Jun. 2016, pp. 1874–1883.

[45] H. Kazemi, F. Taherkhani, and N. M. Nasrabadi, "Identity-aware deep face hallucination via adversarial face verification," 2019, *arXiv:1909.08130*. [Online]. Available: http://arxiv.org/abs/1909.08130
[46] T. Wang, W. Sun, H. Qi, and P. Ren, "Aerial image super resolution via wavelet multiscale convolutional neural networks," *IEEE Geosci. Remote Sens. Lett.*, vol. 15, no. 5, pp. 769–773, May 2018.
[47] A. Radford, L. Metz, and S. Chintala, "Unsupervised representation learning with deep convolutional generative adversarial networks," 2015, *arXiv:1511.06434*. [Online]. Available: http://arxiv.org/abs/1511.06434
[48] T.-Y. Lin, P. Dollár, R. Girshick, K. He, B. Hariharan, and S. Belongie, "Feature pyramid networks for object detection," in *Proc. IEEE Conf. Comput. Vis. Pattern Recognit.*, Jul. 2017, pp. 2117–2125.
[49] K. Simonyan and A. Zisserman, "Very deep convolutional networks for large-scale image recognition," 2018, *arXiv:1409.1556*. [Online]. Available: https://arxiv.org/abs/1409.1556
[50] M. Bosch, C. M. Gifford, and P. A. Rodriguez, "Super-resolution for overhead imagery using DenseNets and adversarial learning," in *Proc. IEEE Winter Conf. Appl. Comput. Vis. (WACV)*, Mar. 2018, pp. 1414–1422.
[51] S. Ren, K. He, R. Girshick, and J. Sun, "Faster R-CNN: Towards real-time object detection with region proposal networks," in *Proc. Adv. Neural Inf. Process. Syst.*, 2015, pp. 91–99.
[52] R. Girshick, "Fast R-CNN," in *Proc. IEEE Int. Conf. Comput. Vis.*, 2015, pp. 1440–1448.
[53] J. Zhong, T. Lei, and G. Yao, "Robust vehicle detection in aerial images based on cascaded convolutional neural networks," *Sensors*, vol. 17, no. 12, p. 2720, 2017.
[54] C. Chen, J. Zhong, and Y. Tan, "Multiple-oriented and small object detection with convolutional neural networks for aerial image," *Remote Sens.*, vol. 11, no. 18, p. 2176, 2019.
[55] M. Mandal, M. Shah, P. Meena, and S. K. Vipparthi, "SSSDET: Simple short and shallow network for resource efficient vehicle detection in aerial scenes," in *Proc. IEEE Int. Conf. Image Process. (ICIP)*, Sep. 2019, pp. 3098–3102.
[56] M. Ju, J. Luo, P. Zhang, M. He, and H. Luo, "A simple and efficient network for small target detection," *IEEE Access*, vol. 7, pp. 85771–85781, 2019.
[57] Z. Wang, E. P. Simoncelli, and A. C. Bovik, "Multiscale structural similarity for image quality assessment," in *Proc. 37th Asilomar Conf. Signals, Syst. Comput.*, vol. 2, 2003, pp. 1398–1402.
[58] Z. Wang and A. C. Bovik, "A universal image quality index," *IEEE Signal Process. Lett.*, vol. 9, no. 3, pp. 81–84, Mar. 2002.
[59] H. R. Sheikh and A. C. Bovik, "Image information and visual quality," *IEEE Trans. Image Process.*, vol. 15, no. 2, pp. 430–444, Feb. 2006.
[60] E. Koester and C. Safak Sahin, "A comparison of super-resolution and nearest neighbors interpolation applied to object detection on satellite data," 2019, *arXiv:1907.05283*. [Online]. Available: http://arxiv.org/abs/1907.05283

MOKTARI MOSTOFA (Student Member, IEEE) was born in Dhaka, Bangladesh, in 1993. She received the B.Sc. degree in electrical and electronics engineering and the M.Sc. degree in communication and signal processing from the University of Dhaka, Bangladesh, in 2016 and 2018, respectively. She is currently pursuing the Ph.D. degree in electrical engineering with West Virginia University, WV, USA.

Since 2018, she has been a Research Assistant with the Deep Learning Lab and doing research with Prof. N. M. Nasrabadi. Her most research interests include the applications of deep learning, machine learning, and image processing.

SYEDA NYMA FERDOUS received the B.S. degree in computer science from the Military Institute of Science and Technology, Bangladesh, in 2013, and the M.Sc. degree in computer science from the Bangladesh University of Engineering and Technology, Bangladesh, in 2017. She is currently pursuing the Ph.D. degree with the Lane Department of Computer Science and Electrical Engineering, West Virginia University (WVU), USA. Her research interests include deep learning, computer vision, image processing, and machine learning.

BENJAMIN S. RIGGAN (Member, IEEE) received the B.S. degree in computer engineering and the M.S. and Ph.D. degrees in electrical engineering from North Carolina State University, in 2009, 2011, and 2014, respectively. After finishing the Ph.D. degree, he was awarded a Postdoctoral Fellowship at the U.S. Army Research Laboratory's Image Processing Branch, where he worked on face recognition. He was a Postdoctoral Fellow of the U.S. Army Research Laboratory. He worked with the Networked Sensing and Fusion Branch, U.S. Army Research Laboratory. He has published many articles and a book, spanning the subjects of handwriting recognition, face recognition, and fusion. His research interests are in areas of biometrics and fusion, which leverage his expertise in image/signal processing, computer vision, and machine learning. He is currently an Assistant Professor with the Department of Electrical and Computer Engineering, University of Nebraska–Lincoln, Lincoln, NE, USA. His current research interests involve cross-spectrum face recognition and spatial–temporal data fusion for target detection/recognition.

NASSER M. NASRABADI (Fellow, IEEE) received the B.Sc.Eng. degree in electrical engineering from the Imperial College of Science and Technology, in 1980, and the Ph.D. degree in electrical engineering from the University of London, London, U.K., in 1984. In 1984, he was with IBM, U.K., as a Senior Programmer. From 1985 to 1986, he was with the Philips Research Laboratory, New York, NY, USA, as a Member of Technical Staff. From 1986 to 1991, he was an Assistant Professor with the Department of Electrical Engineering, Worcester Polytechnic Institute, Worcester, MA, USA. From 1991 to 1996, he was an Associate Professor with the Department of Electrical and Computer Engineering, The State University of New York at Buffalo, Buffalo, NY, USA. From 1996 to 2015, he was a Senior Research Scientist with the U.S. Army Research Laboratory. Since 2015, he has been a Professor with the Lane Department of Computer Science and Electrical Engineering, West Virginia University. His current research interests include image processing, computer vision, biometrics, statistical machine learning theory, sparsity, robotics, neural networks, and image processing. He is a Fellow of the International Society for Optics and Photonics, ARL, and SPIE. He has served as an Associate Editor for the IEEE TRANSACTIONS ON IMAGE PROCESSING, the IEEE TRANSACTIONS ON CIRCUITS, SYSTEMS, AND VIDEO TECHNOLOGY, and the IEEE TRANSACTIONS ON NEURAL NETWORKS.